Microstructure and Tensile Properties of BN/SiC Coated Hi-Nicalon, and Sylramic SiC Fiber Preforms

Ramakrishna T. Bhatt
U.S. Army Research Laboratory, Glenn Research Center, Cleveland, Ohio

Yuan L. Chen
Dynacs Engineering Company, Inc., Brook Park, Ohio

Gregory N. Morscher
Ohio Aerospace Institute, Brook Park, Ohio

National Aeronautics and
Space Administration

Glenn Research Center

March 2001

Available from

MICROSTRUCTURE AND TENSILE PROPERTIES OF BN/SiC COATED Hi-NICALON, AND SYLRAMIC SiC FIBER PREFORMS

Ramakrishna T. Bhatt
U.S. Army Research Laboratory
National Aeronautics and Space Administration
Glenn Research Center
Cleveland, Ohio 44135

Yuan L. Chen
Dynacs Engineering Company, Inc.
Brook Park, Ohio 44142

Gregory N. Morscher
Ohio Aerospace Institute
Brook Park, Ohio 44142

SUMMARY

Batch to batch and within batch variations, and the influence of fiber architecture on room temperature physical and tensile properties of BN/SiC coated Hi-Nicalon and Sylramic SiC fiber preform specimens were determined. The three fiber architectures studied were plain weave (PW), 5-harness satin (5HS), and 8-harness satin (8HS). Results indicate that the physical properties vary up to 10 percent within a batch, and up to 20 percent between batches of preforms. Load-reload (Hysteresis) and acoustic emission methods were used to analyze damage accumulation occurring during tensile loading. Early acoustic emission activity, before observable hysteretic behavior, indicates that the damage starts with the formation of nonbridged tunnel cracks. These cracks then propagate and intersect the load bearing "0°" fibers giving rise to hysteretic behavior. For the Hi-Nicalon preform specimens, the onset of "0°" bundle cracking stress and strain appeared to be independent of the fiber architecture. Also, the "0°" fiber bundle cracking strain remained nearly the same for the preform specimens of both fiber types. TEM analysis indicates that the CVI BN interface coating is mostly amorphous and contains carbon and oxygen impurities, and the CVI SiC coating is crystalline. No reaction exists between the CVI BN and SiC coating.

1. INTRODUCTION

Preforms of SiC fibers are being used as starting material for the fabrication of SiC- and Al_2O_3-based composites. Such composites have potential for high temperature materials applications including for future generations of aircraft engines because of their high temperature strength (refs. 1 and 2). The preforms are generally fabricated by cutting the two-dimensional woven fiber cloth to the required dimensions, stacking the woven cloth, and then depositing interface coating(s) into the cloth assembly by chemical vapor infiltration (CVI). The thickness and composition of the interface coating(s) depends upon the subsequent composite processing method. After CVI SiC infiltration, the preforms are rigid and porous. The interconnected open porosity in the preforms can be filled with matrix by the melt infiltration (MI), sol gel, or polymer infiltration pyrolysis methods.

For the fabrication of SiC/SiC composites by the nonreactive melt infiltration method, the SiC preforms are prepared by first depositing a layer of boron nitride (BN) and then an outer layer of SiC. The BN/SiC coated preforms are subsequently infiltrated with a slurry of silicon carbide particles and then with liquid silicon (ref. 3). This processing method is scalable for the fabrication of complex, near net shape components with minimum damage to the fibers and interface. However, the state-of-the-art SiC/SiC composites show reproducibility and reliability problems which significantly limit their use temperature to 1200 °C (refs. 2 and 3). The poor reproducibility of mechanical properties in this system is possibly due to batch to batch variations in properties of the starting material, i.e., the SiC preforms, or due to poor process control during the melt infiltration. To understand the source of reproducibility and reliability problems, the current study was performed.

The objectives of this study were several: (1), to determine the batch-to-batch variations in room temperature physical and mechanical properties, and microstructure of the SiC preforms typically used for SiC/SiC composites; (2), to determine the influence of fiber architecture on tensile properties; (3) to determine the damage accumulation in the preforms; (4), to suggest the influence of preform characteristics on the processing and properties of the SiC/SiC composites fabricated by the MI approach.

2. EXPERIMENTAL PROCEDURE

The preforms of BN/SiC coated Hi-Nicalon[TM] and Sylramic[TM] SiC fibers were purchased from Honeywell Advanced Composites Inc, Delaware. The Nippon Carbon Company, Japan, and the Dow Corning Company, Midland, fabricated the Hi-Nicalon and Sylramic fibers, respectively. Albany International Techniweave, Inc., Rochester, NY, performed the weaving of the fiber tows into mats. In the case of the Hi-Nicalon SiC fiber preforms three types of weaves namely the plain weave (PW), 5 harness satin (5HS), and 8HS were studied. Whereas in the case of Sylramic SiC preforms, only 5HS weave was investigated. The preforms contained 8 layers of two-dimensional woven SiC fiber mats and each fiber tow in the mat contained a dual layer of ~0.5 μm thick BN followed by a layer of 3 to 5 μm thick SiC. The nominal dimensions of the preforms after CVI coatings were 229- (L) × 152- (W) × 2-mm (T).

The preforms were cut into smaller specimens of dimensions 152- (L) × 12.5- (W) × 2-mm (T) using a diamond impregnated metal bonded cutoff wheel and water based grinding fluid. The cut specimens were degreased and then dried in an oven. The Archimedes and bulk densities of specimens were measured. For Archimedes density measurements, methyl ethyl ketone liquid was used.

To avoid delamination and compressive failure within the grips of the tensile testing machine, the preforms specimens were impregnated with epoxy. Epoxy infiltration was performed in a vacuum chamber at room temperature. The excess epoxy layer present on the surface of the vacuum impregnated specimens was removed by grinding the specimens on a 200-grit emery paper. A few unreinforced epoxy specimens of dimensions similar to that of epoxy infiltrated preform specimens were also prepared and tensile tested to determine their base line tensile properties.

For tensile testing, dog-bone shaped specimens were machined from the epoxy-infiltrated preform specimens by using an ultrasonic SiC slurry impact machine. At each specimen end, two glass fiber-reinforced epoxy tabs of dimensions 37 × 12 × 1-mm were bonded, leaving ~78 mm between grips. A spring-loaded clip-on gauge was attached to the 25-mm length straight section of the dog bone specimen to monitor the displacement during the tensile test. The specimens were tested at room temperature until failure in a servo-controlled tensile testing machine equipped with self-aligning grips at a crosshead speed of 1.3 mm/min.

In some specimens, the damage occuring during tensile deformation was monitored by two different methods: the hysteresis loop and acoustic emission. In the first method, the specimen was initially loaded to a predetermined load level below the stress corresponding to deviation from linearity (DFL) and then fully unloaded. The specimen was then reloaded to a slightly higher load level and unloaded. This procedure was continued until ultimate failure of the specimen. After the test, the maximum loop width was determined for the different peak stress hysteresis loops.

Acoustic emission was recorded with two wide-band (50 kHz to 2.0 MHz), high fidelity sensors (Model [a]1025) that were placed outside the tapered region of the dog-bone specimen. Vacuum grease was used as a couplant, and alligator clamps were used to mount sensors to the specimen. Acoustic emission waveforms were recorded using a 2-channel, Fracture Wave Detector (FWD). The FWD consisted of a computer (Pentium, 233 MHz) with a 12-bit, 30 MHz analog to digital acquisition board. Each sensor was connected to a preamplifier and filter trigger module, which was fed into the computer. The preamplifier was set at 20 dB; the filter signal was amplified 3 dB. The load and strain were also recorded with the FWD computer. The post-test analysis was performed on Wave Detector[TM] software provided by the FWD manufacturer.

For optical microscopy, some of the specimens were mounted in a metallographic mold, ground successively on 40 mm down to 3 mm diamond particle impregnated metal disks, and polished in a vibratory polisher on a micro cloth using a 0.3 mm diamond powder paste.

---

[a]Digital Wave Corporation, Englewood, Colorada.

For transmission electron microscope (TEM) analysis, the preform specimens were sliced using a diamond saw. Subsequently, each specimen was sandwiched between two sacrificial silicon wafers, vacuum degassed and impregnated with epoxy. After curing, the sandwich assembly was sectioned into smaller specimens of dimensions 2.5 × 2 × 0.5 mm. After polishing one of the sides of the 2.5 × 2 mm surface for flatness, the opposite side of the specimen was thinned to electron transparency using tripod-polishing (ref. 4). As polishing progresses, the thickness of the assembly was periodically monitored using a reflected light microscope. As the thickness of the sacrificial silicon wafer decreased, its color also changed. When the color of the sacrificial silicon turned from orange to yellow, the polishing was stopped. Tripod polishing makes it possible to mechanically polish a large area of a very thin specimen with no or minimum mechanical damage. The superficial mechanical damage seen on some specimens was removed by low angle (<7°) argon ion-beam milling for about 10 to 20 min. The present transmission electron microscopy results include imaging and quantitative analyses of the transverse cross-section of the specimens. In this mode, the fibers were observed "end-on." Diffraction contrast and phase contrast images, selected-area, and microdiffraction data were recorded using a Philips CM200 electron microscope operated at 200 kV. The TEM is coupled to an energy dispersive X-ray (EDX) spectrometer for chemical identification.

3. RESULTS AND DISCUSSION

Because of its low viscosity, epoxy uniformly fills the available open pore space in the preform specimens. Typical cross-sections of an epoxy infiltrated 5HS woven BN/SiC coated Hi-Nicalon SiC fiber preform specimens are shown in figure 1. Figure 1(a) indicates that the Hi-Nicalon tows are oblong and show gaps between the fiber tows. A higher magnification photograph of the cross-section (fig. 1(b)) shows that the diameter of the SiC fibers within the tow varies from 10 to 16 μm. The dark ring around the SiC fibers in figure 1(b) is the BN coating. The gray coating on top of the dark ring represents the CVI SiC coating. When fibers are well separated, the BN coating is seen on the fibers, but when fibers clumped together, the BN coating is not visible. Also noticed are a few isolated regions of closed porosity within the coated tows. In many regions, the 0° tow of one ply rests on 0° tow of the adjacent ply and the 90° tow rests on 90° tow with no CVI SiC coating between the tows. Optical examination of the cross-section of the epoxy infiltrated 5HS woven BN/SiC Sylramic SiC fiber preforms indicates that the fibers are tightly packed inside the tows, and have a relatively uniform diameter of ~9 μm, discounting a few smaller diameter fibers. The BN coating is relatively uniform around the fiber, and the thickness of the SiC coating increases from the center to the outer periphery of the tow. On many tows, a thick SiC layer was noticed on the outer periphery, completely surrounding the tows. The coated tows contain nearly 2 to 6 vol % of closed porosity, which is not even accessible for the epoxy infiltration.

The TEM micrographs of the cross-section of the BN/SiC coated Hi-Nicalon and Sylramic SiC fiber preforms are shown in figure 3. In both preforms, the BN coating is mostly amorphous and the SiC coating is crystalline. The SiC coating is composed of columnar grains that are aligned radially around the SiC fibers. In some Hi-Nicalon preform specimens, a graded region of fine grained SiC and BN was noticed between the BN and SiC coating. In contrast, the boundary between the BN and SiC coating is sharp and distinct in the Sylramic SiC preform specimens. Quantitative EDX analysis indicates that the BN coating contains up to 8 percent carbon and oxygen impurities.

The variations in Archimedes and bulk densities, and volume percent open porosity within and between batches of the PW, 5HS, and 8HS woven Hi-Nicalon and 5HS Sylramic SiC preforms were measured. The data for 5HS preforms are shown in figures 4 to 6. In some batches, only one specimen was tested, where as in other batches up to 17 specimens were tested. The scatter band is shown for batches where a statistically significant number of specimens were tested. The scatter band represents two standard deviations. The Archimedes density within a batch is uniform, but between batches, it varies up to 10 percent. This suggests variation in closed porosity or the SiC coating thickness, or both. In fact, the optical micrographs of the cross-section of different batches of preforms show closed porosity variations between 2 and 6 percent, and CVI SiC coating thickness variations from 2 to 5 μm. In contrast, the variations in bulk density and volume percent porosity were significant both within a batch as well as between the batches (figs. 5 and 6). Some of the variation in physical density can be attributed to error in thickness measurement of the preform specimens because of the nodular surface. To minimize the error, the thickness measurements were made at fifteen different locations along the length of the specimen to obtain an average value. The physical property data for the preforms are summarized in table I. The scatter band in the data values represents two standard deviations. The range of values measured is shown in the brackets. When Hi-Nicalon preform specimens are compared, the average Archimedes and physical density values for 5HS are generally higher than the those of

the other two preform specimens, whereas the average pore fraction of 5 HS preform is lower than those of the other two preform specimens. The average Archimedes density values for the PW, 5HS, and 8HS woven Hi-Nicalon preform specimens are generally lower than those for the 5HS woven Sylramic SiC preforms primarily due to the density difference between the Hi-Nicalon-2.74 gm/cc (ref. 5) and Sylramic SiC fibers-3.0 gm/cc (ref. 6). Other noticeable points are that the standard deviation and the difference in extreme values remain nearly the same for both fiber types for the same architecture.

Attempts were made to determine size range of interconnected porosity in the preforms by mercury porosimetry and nitrogen adsorption techniques. In the case of the porosimeter, mercury easily filled the preform at standard temperature and pressure conditions, making further infiltration of mercury under pressure impossible. On the other hand, pore size determination by the adsorption technique could not be used because preform surface repelled nitrogen gas.

The room temperature tensile stress-strain curves for the epoxy infiltrated PW, 5HS, and 8 HS Hi-Nicalon SiC preform specimens are shown in figure 7. For comparison purposes, included in the figure is the stress-strain curve for the unreinforced epoxy. Clearly, the modulus and UTS for the unreinforced epoxy is significantly lower than those for the epoxy infiltrated preform specimens. This suggests that the epoxy matrix does not influence the deformation behavior and tensile properties of the preform specimens. In figure 7, all three weaves displayed similar features on the stress-strain curves: An initial linear region followed by a nonlinear region. The stress corresponding to deviation from linearity (DFL) for the 5HS and PW specimens appears to be the same, but the DFL value for the 8 HS preform specimens is slightly lower than that of the other two weaves. Also noticed is that the UTS of 8HS preform specimens is greater than that of the other weaves, and elastic modulus of the 5HS and PW specimens is nearly the same.

Although ultimate tensile strength and failure strain for the 5HS Sylramic preform specimens are relatively lower than those for the 5HS Hi-Nicalon preform specimens, the stress-strain behavior for the 5HS Sylramic preform specimens exhibited features similar to that of the 5HS Hi-Nicalon preform specimens. Therefore, its stress-strain curve is not shown in figure 7.

Variation of the elastic modulus with open porosity is plotted in figure 8 for the epoxy infiltrated Hi-Nicalon and Sylramic preform specimens. The solid lines in both figures represent the predicted modulus based on rule-of-mixtures with the assumption that transverse tows do not contribute to the modulus. For this calculation the following constituent property values were used: $E_{SiC(Hi-Nicalon)} = 270$ GPa (ref. 5), $E_{SiC(Sylramic)} = 390$ GPa (ref. 6), $E_{(CVD\ BN)} = 62$ GPa (ref. 7), $E_{(CVD\ SiC)} = 425$ GPa (ref. 8) $V_{SiC} = 40\%$, $V_{BN} = 6\%$, and $V_{CVI\ SiC} = 20\%$. For the two fiber types, an inverse relationship between open porosity and elastic modulus was noticed. Also noticed is that for a fixed pore fraction, the predicted modulus value was slightly higher than the measured value. The discrepancy is possibly due to not accounting for 2 to 6 vol % of closed porosity present in the preform specimens when the calculations were made. The inverse relationship seen here between porosity and elastic modulus is consistent with CVI literature (refs. 9 and 10). Previous studies indicate that in the early stages of CVI in stacked plies of fibers, the open porosity decreases, and the tortuosity of interconnected pores changes continuously, but beyond a critical level of deposition increasing amounts of closed porosity are also formed (refs. 9 and 10).

Table II summarizes the room temperature tensile property data for the four SiC preforms and the unreinforced epoxy matrix. Each data entry and the corresponding standard deviation in the table represent an average of 7 tests. The following conclusions can be drawn from the comparison of the data shown in the table. First, fiber architecture had no effect on the tensile properties of the Hi-Nicalon preforms. Second, the stress or strain corresponding to the DFL remained nearly the same for all four preforms irrespective of fiber architecture and fiber composition. Third, primary elastic modulus of Sylramic SiC preforms is higher than that of the Hi-Nicalon SiC preforms. Fourth, the Hi-Nicalon SiC preforms show significantly higher ultimate strength and strain than the Sylramic SiC preforms.

Figure 9 shows the static and hysteresis stress-strain curves of 5HS Hi-Nicalon specimen. The static and hysteresis stress-strain curves are almost identical. The hysteresis stress-strain curves have slightly larger strains for the same stress compared to the static stress-strain curve. The onset of $0°$ fiber bundle cracking is considered to occur when the hysteresis loop width is >0. With increasing stress, the specimen upon unloading showed increasing amounts of residual strain and increasing loop widths. This indicates progressive damage in the form of bridged matrix cracks with increasing applied stress in the preform until failure. The variation of maximum loop width with peak stress is shown in figures 10 and 11, respectively, for the PW, 5HS, and 8HS Hi-Nicalon and 5HS Sylramic SiC preform specimens.

The onset of "0°" cracking was determined by extrapolating the hysteresis loop width versus stress or strain to a value of zero stress or strain, respectively. This occurred for a stress and strain of ~90 MPa and ~0.075 to 0.08 percent, respectively, for all the preforms tested. In other words, there was no discernable effect of architecture or fiber type on the hysteresis behavior. This suggests that the "0°" cracking stress and strain is invariant and is controlled by the CVI SiC coating. It should be noted that for Hi-Nicalon and Sylramic reinforced CVI and/or MI SiC matrix composites, the onset stress for 0° cracking is higher for higher elastic modulus composites. However, the onset strain for all the SiC/SiC composites, ~0.075 percent, was about the same as the epoxy infiltrated composites (refs. 11).

The AE results are shown in figure 12 plotted as normalized cumulative AE energy versus strain. The data pertains to the stress strain data of figure 9 and other hysteresis tensile tests not shown. Normalized cumulative AE energy is determined by summing the AE event energies in chronological order of events and then normalizing that data by the absolute cumulative AE energy of all events. There are two reasons for analyzing the AE data in this manner. First, AE energy has been shown to be the best parameter relating to matrix damage (refs. 12 and 13). Second, the absolute AE energy (and number of events) can vary by a factor of two due primarily to sensor contact. However, the relative (normalized) amounts of AE activity are comparable from specimen to specimen. Also, the onset of AE activity usually occurs at stresses lower than any nonlinearity in the stress-strain curve (refs. 14 and 15), and is a good indicator of first cracking in the material that is usually in the form of nonbridging tunnel cracks (refs. 11 and 16).

The data plotted in figure 12 are for hysteresis tensile tests. Some events occurred during unloading and subsequent reloading. These correspond to the sharp decreases in strain for AE data in figure 12. This is very common for hysteresis type testing and is indicative of some damage occurring during unloading and reloading (ref. 17). The onset of AE activity occurs at ~0.04 percent (~40 to 50 MPa) for all the preforms tested. Interestingly, the strain for initial AE activity for a CVI SiC matrix composite, also shown in figures 9 and 12, occurs at 0.025 percent, even less than for the preforms; however, the stress for initial AE activity occurs at ~50 MPa, about the same as for the preforms. Since initial cracking occurs at stresses well below the formation of hysteresis loops, the first cracks are presumably nonbridging tunnel cracks (ref. 16). The first cracks in CVI SiC matrix composites have been shown to emanate from the sharp large pores formed where 90° and 0° bundles meet (ref. 11, 18 to 21). Presumably, the same is true for the preforms, since the stress to initiate first matrix cracking is the same for preforms as for CVI matrix composites. Figures 13 and 14 show typical tensile fracture surfaces of epoxy infiltrated 5HS BN/SiC coated Hi-Nicalon and Sylramic SiC preform specimens. Comparison of figures 13 and 14 indicates several differences in the fracture behavior of two types of preforms. The fracture surface of the Hi-Nicalon preform specimen shows extensive fiber pullout throughout the cross-section. However, the fracture surface of Sylramic SiC preform specimen shows brittle/flat fracture in some regions and tow pullout in other regions. The fiber tows appeared to be sintered together and show staggered fractures. A higher magnification photograph of the brittle fracture region indicates fiber to fiber contact with little or no BN coating around the SiC fibers.

In summary, open porosity varies between 20 to 45 vol %, between batches of the preforms of BN/SiC Hi-Nicalon and Sylramic SiC fiber and closed porosity varies between 2 to 6 vol %. This large variation in open porosity is caused by thickness or volume fraction variation of the CVI SiC coating. Variation of porosity and volume fraction of CVI SiC coating will influence both processing parameters and properties of the SiC/SiC composites fabricated by the MI approach. From the processing point of view, it is difficult to formulate a slurry that can fully infiltrate into a preform containing such a wide variation in porosity, pore size distribution, and tortuosity. Consequently, some preforms can be fully infiltrated with the slurry and others can contain voids due to choking of the slurry at the pore neck. These voids cannot be filled with silicon during the final MI step because of capillary and surface tension forces. From the property point of view, voids and porosity are known to decrease the modulus, transverse thermal conductivity, and interlaminar tensile strength of composites. In contrast, the variation in volume fraction of CVI SiC coating may or may not affect properties of a fully dense SiC/SiC composite depending on the relative differences in the properties of the MI SiC matrix and the CVI SiC coating. If the properties of MI SiC matrix are similar to that of the CVI SiC coating, then variation in volume fraction of CVI SiC coating in the preform may not affect the properties of the SiC/SiC composites. In other cases, they would. In conclusion, the results of this study indicate better control in thickness of the CVI SiC coating and the porosity of the BN/SiC coated SiC preforms is needed to improve reproducibility and reliability of SiC/SiC composites.

4. SUMMARY OF RESULTS

The room temperature properties, damage accumulation, and microstructure of BN/SiC coated Hi-Nicalon and Sylramic SiC fiber preforms were characterized. The influence of fiber architecture on properties was investigated. Key findings are the following.

1. The variation in Archimedes, and physical densities, and pore fraction is much greater between the batches (~20 percent) compared to within a batch (~10 percent) for the BN/SiC coated Hi-Nicalon SiC and Sylarmic SiC fiber preform specimens.

2. Both Hi-Nicalon SiC and Sylarmic SiC fiber preforms show an inverse relationship between the modulus and pore fraction.

3. Fiber architecture has no effect on the room temperature tensile properties of the Hi-Nicalon preforms.

4. Fiber architecture and fiber modulus have no effect on first matrix cracking, or the onset stress and strain of cracks which are bridged by the fibers, i.e., "0°" bundle cracks.

5. As the fiber modulus increased so did the "0°" bundle cracking stress.

6. In Sylramic SiC fiber preforms, there is no chemical reaction between the BN and SiC layers, but in Hi-Nicalon SiC preforms, a graded region of small grained SiC and BN was observed between the layers. The BN interface is amorphous and the SiC grains are columnar.

REFERENCES

1. M. Johnson, B.J. Bartlett, and W.A. Troha, Proceedings of the 13th International Symposium on Air Breathing Engines, Chattanooga, Tennessee, U.S.A., 1997, edited by S. Billing, Vol. II, ISABE 97–7179, p. 1321.
2. D. Brewer, Mat. Sci. and Eng., **A261** (1999) 284.
3. S.K. Lau, S.J. Calandra, and R.W. OHNSORG, US Pat. 5,840,221, 1998.
4. J.P. Benedict, S.J. Klepeis, and R. Anderson, Proceedings: Microscopy and Microanalysis, Cleveland, Ohio (August 1997), edited by 3, (2), (Springer-Verlag, New York Inc., 1987) 339.
5. M. Takeda, Y. Imai, H. Ichikawa, T. Ishikawa, N. Kasai, T. Seguchi, and K. Okamura, Ceram. Eng. Sci. Pro, **12** (1991) 1007.
6. J. Lipowitz, J.A. Rabe, A. Zangvil, and Y. Xu, Ceram. Eng. Sci. Pro, **18** (1997) 147.
7. "Engineering Property Data on Selected Ceramics, Vol I, Nitrides" Report # MCIC-HB-07, (1976) Metals and Ceramics Information Center, Battelle Columbus Laboratories, Columbus, OH.
8. J.S. Goela, M.A. Pickering, R.L. Taylor, B.W. Murray and A. Lompado, Appl. Opt. **30** (1991) 3166.
9. W.J. Lacyey and T.L. Starr, " Fiber-Reinforced Ceramic Composites: Materials, Processing, and Technology edited by K.S. Mazdiyasni (Noyes Publications, Park Ridge, New Jersey, U.S.A, 1990) p. 347.
10. P.J. Geoghegan, "Flight-Vehicle Materials, Structure, and Dynamics- Assessment and Future Directions" edited by A.H. Noor, and S.L. Venneri, The American Society of Mechanical Engineers, 345 East 47th Street, United Engineering Center, New York, NY 10017, 1992) p. 113.
11. G.N. Morscher, J.Z. Gyekenyesi, and R.T. Bhatt, "Mechanical, Thermal, and Environmental Properties and Performance of Ceramic Composites and Components" ASTM STP 1392 edited by M.G. Jenkins, E. Lara-Curzio, and S.T. Gonczy, (American Society for Testing and Materials, West Conshohocken, PA, 2000) p. 306.
12. G.N. Morscher, and J.Z. Gyekenesi, Ceram. Eng. Sci. Proc. **19**[3], (1998) 241.
13. G.N. Morscher, Comp. Sci. Tech. **59**[5], (1999) 687.
14. R.Y. Kim, and N.J. Pagano, J. Amer. Ceram. Soc. **74**[5], (1991) 1082.
15. Y-J. Luo, S.C. Chang, and I.M. Daniel, J. Comp. Mat. **29**, (1995) 1946.
16. B.N. Cox, and D.B. Marshall, J. Amer. Ceram. Soc. **79**[5], (1996) 1181.
17. M.G. Jenkins, J.P. Piccola, and E. Lara-Curzio, in "Fracture Mechanics of Ceramics," **12**, Edited by R.C. Bradt, D.P.H. Hasselman, D. Munz, M. Sakai, and V.Y. Shevchenko (Plenum Publishing Corp., USA, 1996) p. 267.
18. G.N. Morscher, in "Review of Progress in Quantitative Nondestructive Evaluation," **19**, Edited by D.O. Thompson and D.E. Chimenti (Kluwer Academic/Plenum Publishers) in print.
19. L. Guillaumat, and J. Lamon, in "Revue Des Composites et Des Materiaux Advances," **3**, (1993) p. 159.
20. L. Guillaumat, and J. Lamon, Comp. Sci. Tech. **56** (1996) 803.
21. P. Pluvinage, A. Parvizi-Majidi, and T.W. Chou, J. Mat. Sci. **31**, (1996) 232.

TABLE I.—PHYSICAL PROPERTIES OF BN/SIC COATED HI-NICALON AND
SYLRAMIC SIC FIBER PREFORMS

Fiber	Weave	# Tested specimens	Archimedes density, gm/cc	Physical density, gm/cc	Pore fraction
Hi-Nicalon	PW	19	2.71±0.02 [a](2.67 – 2.73)	1.63±0.14 [a](1.47 – 1.87)	0.40±0.05 [a](0.31 – 0.46)
Hi-Nicalon	5HS	57	2.79±0.03 [a](2.67 – 2.83)	2.08±0.19 [a](1.69 – 2.29)	0.26±0.06 [a](0.19 – 0.41)
Hi-Nicalon	8HS	11	2.68±0.12 [a](2.54 – 2.79)	1.74±0.20 [a](1.46 – 1.95)	0.35±0.05 [a](0.30 – 0.43)
Sylramic	5HS	79	2.91±0.04 [a](2.77 – 2.95)	1.86±0.13 [a](1.59 – 2.18)	0.36±0.05 [a](0.25 - 0.45)

[a]Indicate range of values.

TABLE II.—ROOM TEMPERATURE TENSILE PROPERTY DATA FOR
EPOXY, AND EPOXY INFILTRATED BN/SIC COATED HI-NICALON AND
SYLRAMIC SIC FIBER PREFORMS

Preform	Weave	DFL stress, MPa	DFL strain, percent	E, GPa	Ultimate tensile stress, MPa	Ultimate tensile strain, percent
Epoxy	None	– – – –	– – – – –	3±0.13	8±0.69	0.27±0.03
Hi-Nicalon	PW	63±14	0.06±0.005	113±22	352±50	0.86±0.12
Hi-Nicalon	5HS	71±12	0.06±0.02	124±24	370±32	0.74±0.07
Hi-Nicalon	8HS	81±10	0.09±0.02	93±12	405±29	0.83±0.08
Sylramic	5HS	75±14	0.05±0.02	135±30	196±31	0.23±0.03
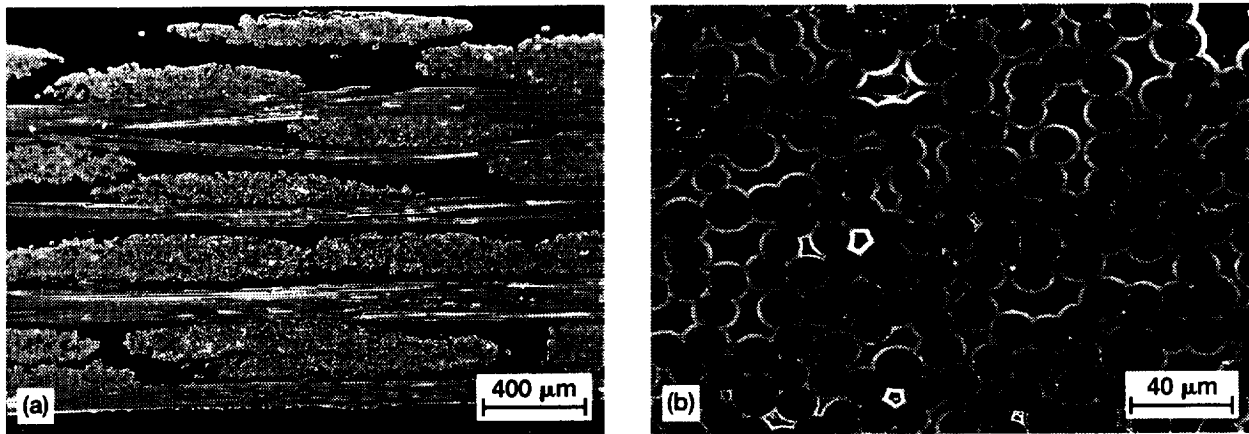
Figure 1.—Optical photographs of the cross-section of epoxy infiltrated BN/SiC coated Hi-Nicalon SiC preforms showing tow distribution and fiber distribution within a tow.
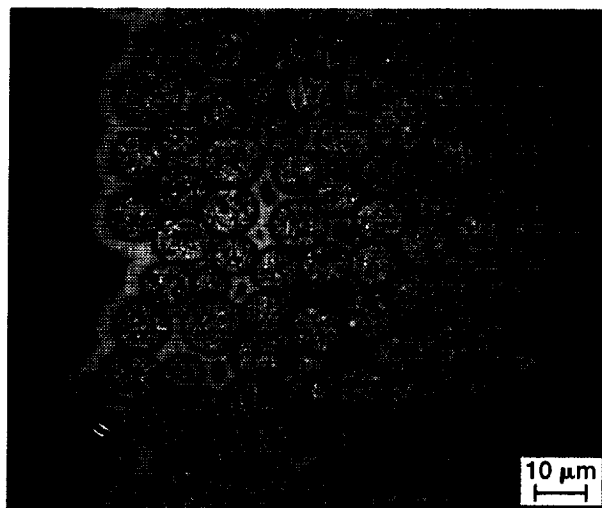
Figure 2.—Optical photograph of the cross-section of epoxy infiltrated BN/SiC coated Sylramic SiC preforms showing tow distribution and CVD coating thickness variation within a tow.
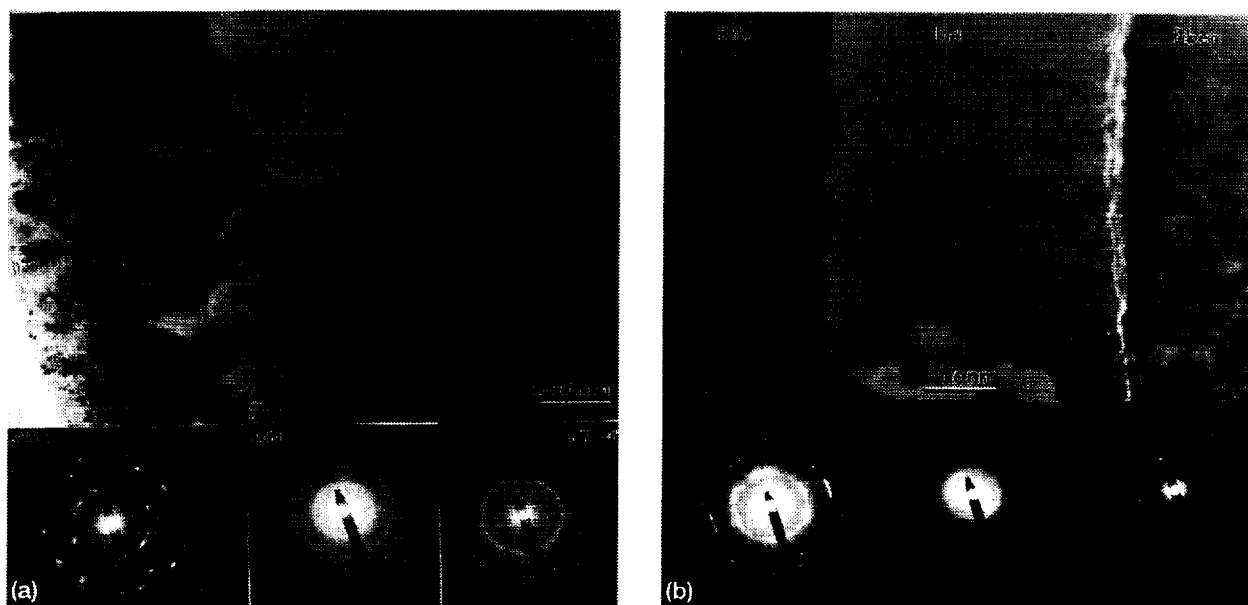
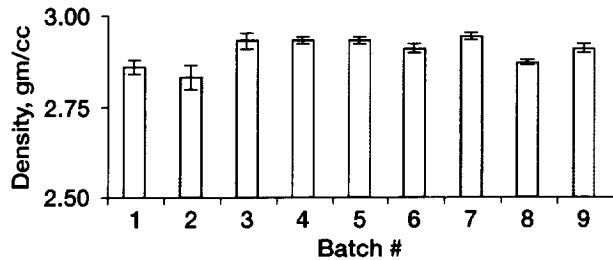Figure 3.—TEM micrographs of the interface regions of BN/SiC coated SiC fiber prefoms: (a) Hi-Nicalon (b) Sylramic.
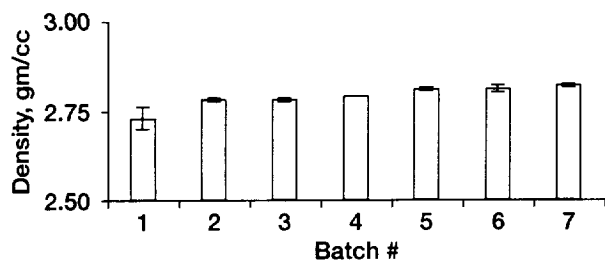
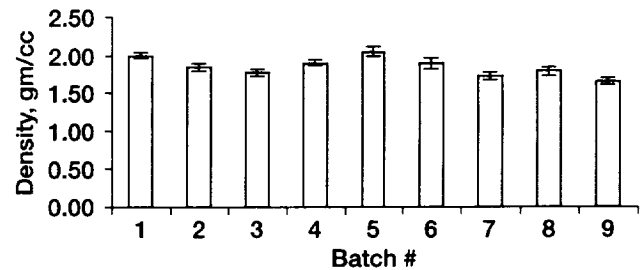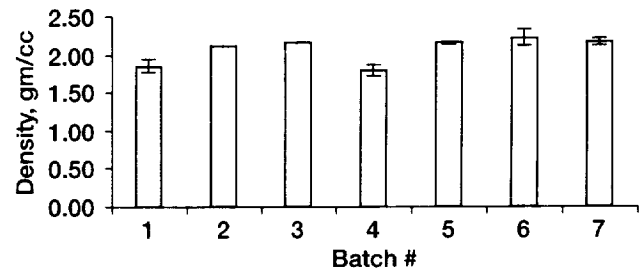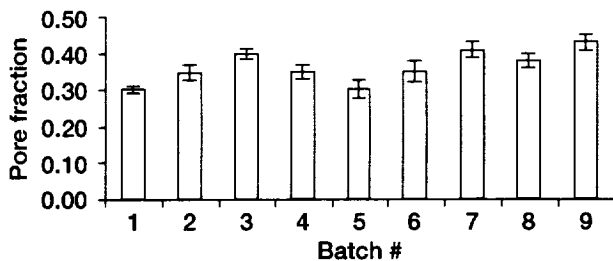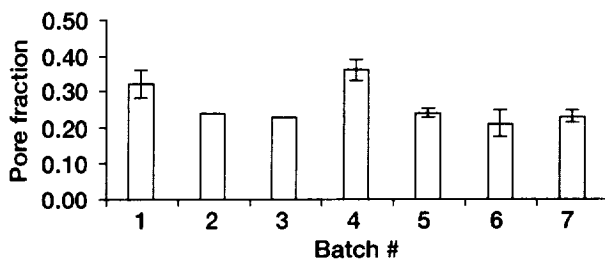Figure 4.—Batch to batch variation in Archimedes density for BN/SiC coated Hi-Nicalon and Sylramic SiC preforms.

Figure 5.—Batch to batch variation in physical density for BN/SiC coated Hi-Nicalon and Sylramic SiC preforms.

Figure 6.—Batch to batch variation in open porosity for BN/SiC coated Hi-Nicalon and Sylramic SiC preforms.
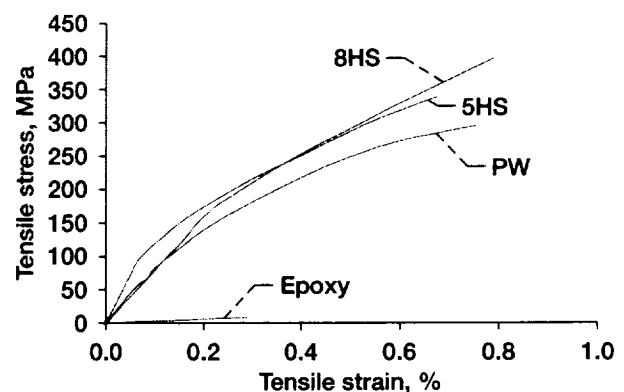
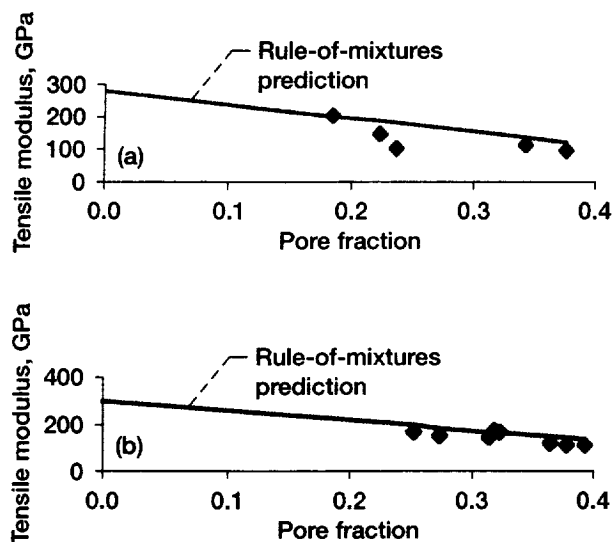Figure 7.—Room temperature tensile stress-strain curves for epoxy and epoxy infiltrated PW, 5HS, and 8HS BN/SiC coated Hi-Nicalon SiC fiber preforms.

Figure 8.—Variation of room temperature tensile modulus with pore fraction for BN/SiC coated SiC fiber preforms: (a) Hi-Nicalon, (b) Sylramic.
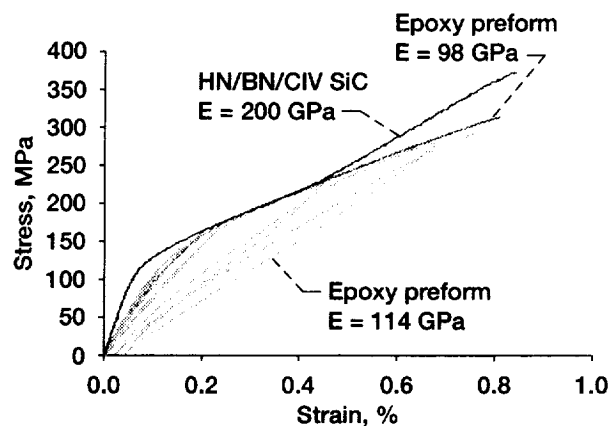

Figure 9.—Typical unload-reload hysteresis curve for epoxy infiltrated 5HS Hi-Nicalon SiC preforms and a CVI SiC/SiC composite.
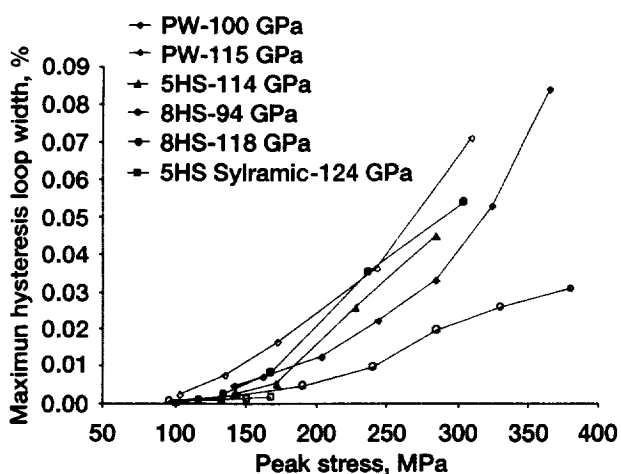

Figure 10.—Maximum hysteresis loop width versus peak stress for various epoxy infiltrated BN/SiC coated Hi-Nicalon and Sylramic SiC preforms.
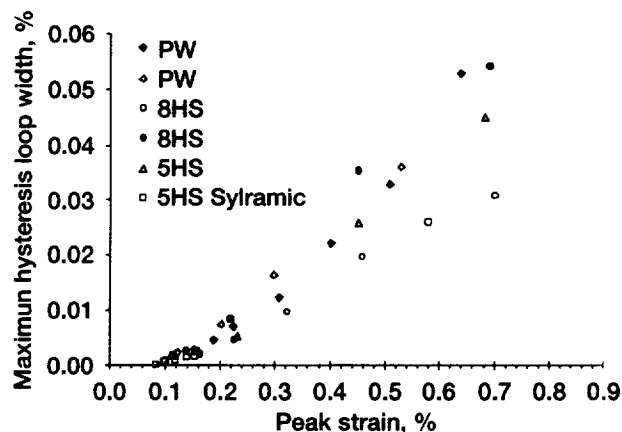

Figure 11.—Maximum hysteresis loop width versus peak strain for various epoxy infiltrated BN/SiC coated Hi-Nicalon and Sylramic preforms.
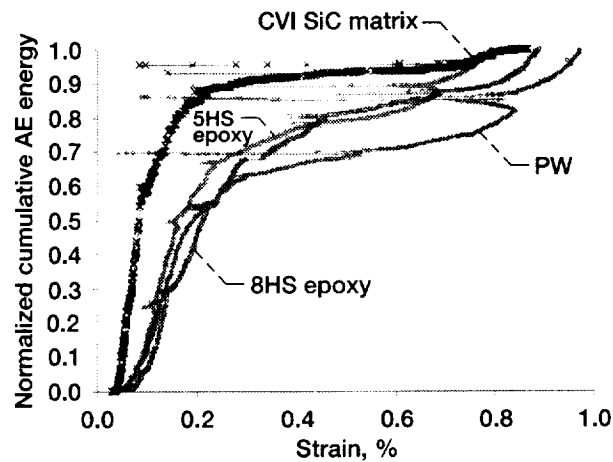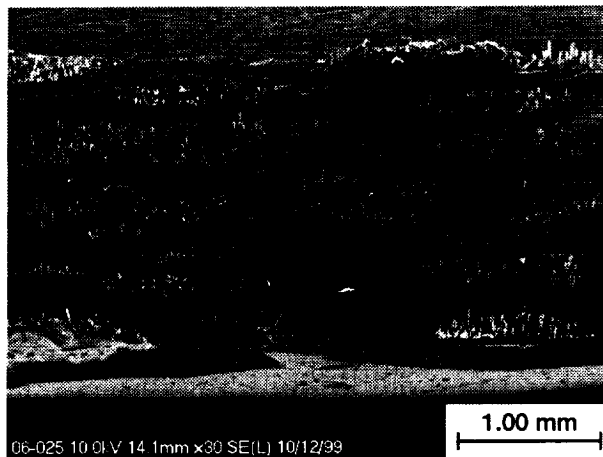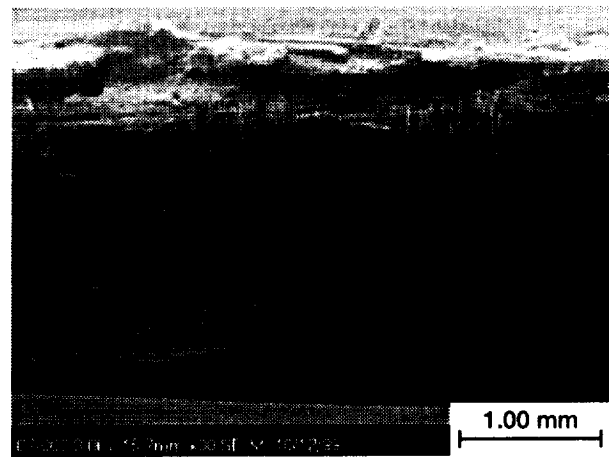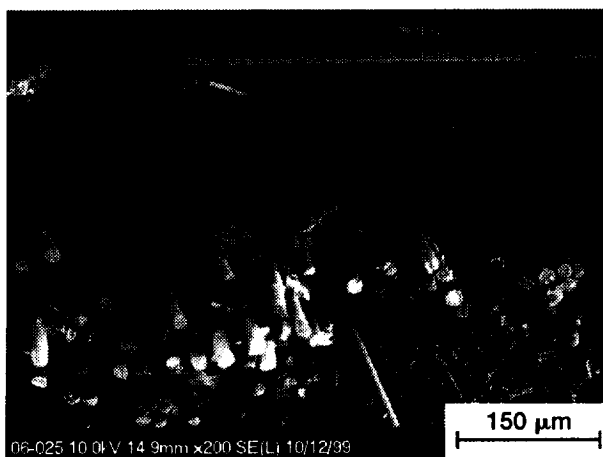
Figure 12.—Comparison of AE cumulative energy with loading for epoxy infiltrated 8HS Hi-Nicalon SiC preforms and 8HS Hi-Nicalon SiC/SiC composites.

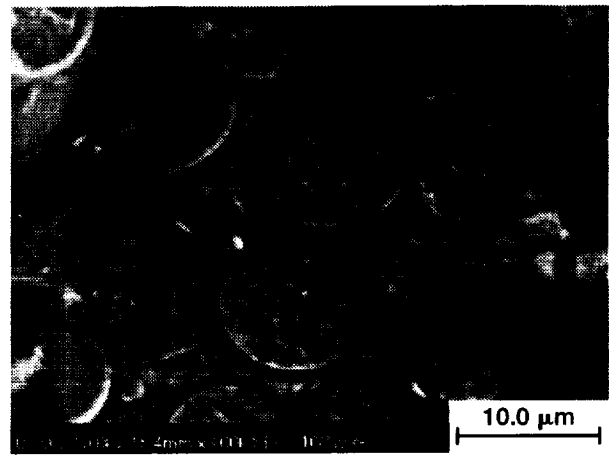Figure 13.—SEM photographs of the tensile fracture surfaces of epoxy infiltrated 5HS woven Hi-Nicalon SiC preforms showing (a) failure across the specimen, and (b) fiber pull out within a tow.

Figure 14.—SEM photographs of the tensile fracture surfaces of epoxy infiltrated 5HS woven Sylramic SiC preforms showing (a) brittle and pullout regions and (b) fiber to fiber contact in the brittle region.

REPORT DOCUMENTATION PAGE		Form Approved OMB No. 0704-0188

Public reporting burden for this collection of information is estimated to average 1 hour per response, including the time for reviewing instructions, searching existing data sources, gathering and maintaining the data needed, and completing and reviewing the collection of information. Send comments regarding this burden estimate or any other aspect of this collection of information, including suggestions for reducing this burden, to Washington Headquarters Services, Directorate for Information Operations and Reports, 1215 Jefferson Davis Highway, Suite 1204, Arlington, VA 22202-4302, and to the Office of Management and Budget, Paperwork Reduction Project (0704-0188), Washington, DC 20503.

1. AGENCY USE ONLY (Leave blank)	2. REPORT DATE March 2001	3. REPORT TYPE AND DATES COVERED Technical Memorandum	
4. TITLE AND SUBTITLE Microstructure and Tensile Properties of BN/SiC Coated Hi-Nicalon, and Sylramic SiC Fiber Preforms			**5. FUNDING NUMBERS** WU–714–04–30–00
6. AUTHOR(S) Ramakrishna T. Bhatt, Yuan L. Chen, and Gregory N. Morscher			
7. PERFORMING ORGANIZATION NAME(S) AND ADDRESS(ES) National Aeronautics and Space Administration John H. Glenn Research Center Cleveland, Ohio 44135–3191			**8. PERFORMING ORGANIZATION REPORT NUMBER** E–12626
9. SPONSORING/MONITORING AGENCY NAME(S) AND ADDRESS(ES) National Aeronautics and Space Administration Washington, DC 20546–0001			**10. SPONSORING/MONITORING AGENCY REPORT NUMBER** NASA TM—2001-210695

11. SUPPLEMENTARY NOTES

Ramakrishna T. Bhatt, U.S. Army Research Laboratory, Glenn Research Center; Yuan L. Chen, Dynacs Engineering Company, Inc., 2001 Aerospace Parkway, Brook Park, Ohio 44142; and Gregory N. Morscher, Ohio Aerospace Institute, 22800 Cedar Point Road, Brook Park, Ohio 44142. Responsible person, Ramakrishna T. Bhatt, organization code 0300, 216–433–5513.

12a. DISTRIBUTION/AVAILABILITY STATEMENT	12b. DISTRIBUTION CODE
Unclassified - Unlimited Subject Category: 24 Distribution: Nonstandard Available electronically at http://gltrs.grc.nasa.gov/GLTRS This publication is available from the NASA Center for AeroSpace Information, 301–621–0390.	

13. ABSTRACT (Maximum 200 words)

Batch to batch and within batch variations, and the influence of fiber architecture on room temperature physical and tensile properties of BN/SiC coated Hi-Nicalon and Sylramic SiC fiber preform specimens were determined. The three fiber architectures studied were plain weave (PW), 5-harness satin (5HS), and 8-harness satin (8HS). Results indicate that the physical properties vary up to 10 percent within a batch, and up to 20 percent between batches of preforms. Load-reload (Hysteresis) and acoustic emission methods were used to analyze damage accumulation occurring during tensile loading. Early acoustic emission activity, before observable hysteretic behavior, indicates that the damage starts with the formation of nonbridged tunnel cracks. These cracks then propagate and intersect the load bearing "0°" fibers giving rise to hysteretic behavior. For the Hi-Nicalon preform specimens, the onset of "0°" bundle cracking stress and strain appeared to be independent of the fiber architecture. Also, the "0°" fiber bundle cracking strain remained nearly the same for the preform specimens of both fiber types. TEM analysis indicates that the CVI BN interface coating is mostly amorphous and contains carbon and oxygen impurities, and the CVI SiC coating is crystalline. No reaction exists between the CVI BN and SiC coating.

14. SUBJECT TERMS Microstructure; Physical and tensile properties; SiC preforms; TEM; BN/SiC coated SiC preforms; Mechanical properties; Acoustic emission			15. NUMBER OF PAGES 17
			16. PRICE CODE A03
17. SECURITY CLASSIFICATION OF REPORT Unclassified	**18. SECURITY CLASSIFICATION OF THIS PAGE** Unclassified	**19. SECURITY CLASSIFICATION OF ABSTRACT** Unclassified	**20. LIMITATION OF ABSTRACT**

NSN 7540-01-280-5500

Standard Form 298 (Rev. 2-89)
Prescribed by ANSI Std. Z39-18
298-102